

Contact-induced negative differential resistance in short-channel graphene FETs

Roberto Grassi, *Member, IEEE*, Tony Low, Antonio Gnudi, *Member, IEEE*,
and Giorgio Baccarani *Fellow, IEEE*

Abstract—In this work, we identify a physical mechanism for the phenomenon of negative output differential resistance (NDR) in short-channel graphene FETs (GFETs) through non-equilibrium Green's function (NEGF) simulations. This NDR phenomenon is due to a transport mode bottleneck effect induced by the source and drain contacts, which we further elucidate using a simpler semianalytical ballistic model that captures the essential physics. This NDR effect is found to occur only when the gate biasing produces an n-p-n or p-n-p polarity configuration along the channel, for both positive and negative drain-source voltage sweep. In addition, we also explore the impact on the NDR effect of contact-induced energy broadening in the source and drain regions and a finite contact resistance.

I. INTRODUCTION

GRAPHENE has attracted considerable interest in recent years for applications in analog radio frequency (RF) electronics [1]–[4]. The reason lies in the fact that the high carrier mobility and Fermi velocity of graphene could allow device operation up to the THz range of frequencies, while the small on-off current ratio resulting from the zero bandgap, which currently prevents the use of graphene in digital electronics, does not pose a problem in principle for analog applications [5]. Indeed, an integrated RF circuit made of graphene devices has already been demonstrated [6]. However, in more general analog circuits, devices with current saturation, i.e. small output conductance g_d , are usually required. This is because the intrinsic voltage gain g_m/g_d , where g_m is the device transconductance, must be large. Unfortunately, current saturation in graphene devices is not easily obtained due to the lack of a bandgap.

A quasi-saturation of the output characteristics has actually been reported for some experimental long-channel devices [7]–[9]. This quasi-saturation is commonly attributed to a charge “pinch-off” effect due to the crossing of the quasi-Fermi level with the channel potential [7], [10]–[13]. Recent experiments have shown that not just quasi-saturation ($g_d \rightarrow 0$) but also negative differential resistance ($g_d < 0$) is possible [14], [15]. Indeed, the NDR effect can also be explained with a simple charge “pinch-off” argument [14] within a diffusive transport framework, where the quasi-saturation arises as a particular case. Hence, understanding the origin of NDR is crucial to the engineering of g_d in graphene.

R. Grassi, A. Gnudi, and G. Baccarani are with E. De Castro Advanced Research Center on Electronic Systems (ARCES), University of Bologna, 40136 Bologna, Italy (e-mail: rgrassi@arces.unibo.it).

T. Low is with IBM T.J. Watson Research Center, Yorktown Heights, New York 10598, USA.

In this work, we identify a different physical mechanism for NDR due to the role of contacts, for short-channel graphene transistors operating in the ballistic regime. Indeed contacts [16] were recently found to dominate transport properties of graphene transistors in the ballistic regime. Although there have been quantum transport studies of the NDR effect in the ballistic regime [17]–[19], its origin was not completely elucidated, in particular with regard to the effect of contacts and self-consistent electrostatics, which we found to play an important role in the operating regimes of NDR. It is the purpose of this work¹ to clarify the origin of NDR in ballistic GFETs and provide guidance to future experiments.

The paper is organized as follows. Section II reviews the current interpretations of the quasi-saturation in long- and short-channel GFETs, which prepares the ground for understanding the mechanism behind NDR. Then, Section III describes our simulation models for GFETs. The results are shown in Section IV, followed by a discussion in Section V. Conclusions are finally drawn in Section VI.

II. REVIEW OF QUASI-SATURATION AND NDR IN LONG- VS. SHORT-CHANNEL GFETs

For long-channel GFETs, the phenomenon of quasi-saturation and NDR can be explained using drift-diffusion models, which assume semiclassical diffusive transport [7], [10], [11]. The physical picture is sketched in Fig. 1a: electrons and holes are assumed to be described by a single quasi-Fermi level $E_F(x)$, a function of the position x along the channel; assuming a thin gate oxide, the position in energy of the Dirac point in the channel region E_d follows the gate-source voltage V_{GS} (we neglect the fact that also E_d varies with position), while the drain-source voltage V_{DS} is responsible for the bending of $E_F(x)$ from the Fermi level in the source μ_S to the Fermi level in the drain μ_D . The drain current I is given by

$$I = q [n(x) + p(x)] v(x) W, \quad (1)$$

where q is the electronic charge, $n(x)$ and $p(x)$ the sheet concentration of electrons and holes respectively, $v(x)$ the common drift velocity along the transport direction, and W

¹This paper is an extended version of [20]. It contains new results pertaining to the possibility of NDR in the negative V_{DS} regime, the effect of contact-induced energy broadening [19] and contact resistance, the latter being likely the reason why experimental short-channel devices show only weak NDR [14].

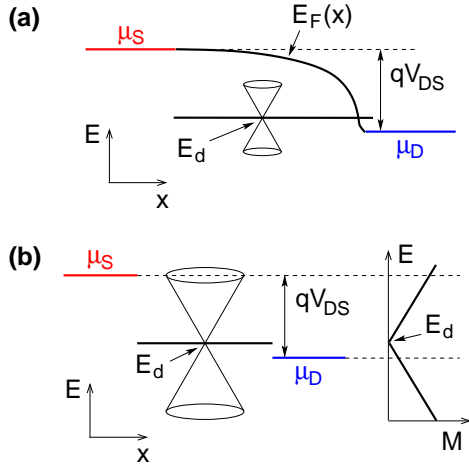


Fig. 1. Band profile in a GFET in the diffusive (a) and ballistic (b) regimes. The cones represent the graphene dispersion relation $E(\vec{k}) = E_d \pm \hbar v_F |\vec{k}|$ and are used to indicate the position in energy of the Dirac point E_d . Also shown in (b) is the plot of $M(E)$. In both the diffusive and ballistic cases, quasi-saturation occurs when the drain Fermi level crosses the channel Dirac point.

the channel width. The output conductance then consists of two contributions:

$$g_d = \frac{\partial I}{\partial V_{DS}} \propto \frac{\partial [n(x) + p(x)]}{\partial V_{DS}} v(x) + [n(x) + p(x)] \frac{\partial v(x)}{\partial V_{DS}}. \quad (2)$$

While $v(x)$ generally increases with V_{DS} due to the increasing bending of the quasi-Fermi level, the sum $[n(x) + p(x)]$ instead is decreasing when $E_F(x)$ approaches and eventually crosses E_d at the drain side. This charge "pinch-off" is the effect used to explain the quasi-saturation in the diffusive regime. It is also possible that velocity saturation, due to scattering with substrate polar phonons, contribute to quasi-saturation [7], [21], since it implies $\partial v(x)/\partial V_{DS} \rightarrow 0$ in the second term in the r.h.s. of Eq. 2. However, there is no clear consensus regarding the velocity saturation effect at present [8]. In addition, the sign of g_d as given by Eq. 2 can actually be negative if the first term prevails over the second. Indeed, the same arguments used for explaining quasi-saturation in long-channel devices can also explain NDR [14].

For ballistic GFETs instead, quasi-saturation can be understood using the Landauer formalism [12] (Fig. 1b). Assuming for simplicity the zero-temperature approximation, the energy window for transport is the one between μ_D and μ_S and the current is given by

$$I = \frac{2q}{h} \int_{\mu_D}^{\mu_S} M(E) dE, \quad (3)$$

where h is Planck's constant, $M(E) = 2W |E - E_d| / (\pi \hbar v_F)$ the number of propagating modes in the graphene channel at energy E , $\hbar = h/(2\pi)$, and v_F the graphene Fermi velocity. In this case, the output conductance is

$$g_d = \frac{\partial I}{\partial V_{DS}} \propto qM(\mu_D) + \int_{\mu_D}^{\mu_S} \frac{\partial M(E)}{\partial V_{DS}} dE. \quad (4)$$

$M(E)$ is shifted up or down in energy by varying E_d , which in turn is determined by the gate electrostatics. Assuming that

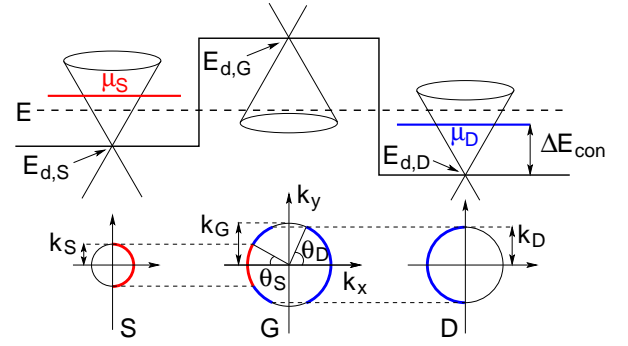


Fig. 2. Semianalytical model: Dirac point profile (top) and population of states in k -space (bottom) corresponding to the indicated energy E . States populated with the Fermi function of the source/drain are indicated with a thick red/blue (light-gray/dark-gray) line.

E_d does not depend on V_{DS} , the second term in the r.h.s. of Eq. 4 is zero. Consequently, it can be seen that the current tends to saturate when μ_D approaches the Dirac point in the channel because $M(E_d) = 0$ (here we neglect the graphene minimum conductivity [22], [23]). The sign of g_d in Eq. 4 can be negative only if $\partial M(E)/\partial V_{DS}$ is negative, which is not obvious from this simple picture. In the following, we will generalize this simple model to include the effects of contacts and self-consistent electrostatics, and show that $\partial M(E)/\partial V_{DS}$ can indeed be negative within the energy window for transport.

III. MODELS

In this section, we describe in detail the semianalytical model and the numerical model which are used to investigate the device behavior.

The semianalytical model assumes a simple ideal square potential barrier, as shown in Fig. 2-top, where $E_{d,S/D/G}$ is the energy of the Dirac point in the source/drain/channel region. This approximation neglects the tunneling probability effect due to the finite transition length of the step potential [24], [25], which is accounted for in the numerical treatment later. Metal induced doping [26] is introduced through a fixed difference ΔE_{con} between the Fermi level and the Dirac point in the metal-doped source and drain regions (Fig. 2-top).

The transport model is composed of the following equations for the electron and hole concentration in the channel region and for the drain current:

$$n = \int_{E_{d,G}}^{\infty} dE [D_L(E) f_S(E) + D_R(E) f_D(E)], \quad (5)$$

$$p = \int_{-\infty}^{E_{d,G}} dE [D_L(E) (1 - f_S(E)) + D_R(E) (1 - f_D(E))], \quad (6)$$

$$I = \frac{2q}{h} \int_{-\infty}^{\infty} dE M(E) [f_S(E) - f_D(E)], \quad (7)$$

where $D_{L/R}(E)$ is the density of states (DOS) in the channel at energy E relative to injection from source/drain and $f_{S/D}(E)$ the contact Fermi distribution with Fermi level $\mu_{S/D}$. In turn, the model for $D_L(E)$, $D_R(E)$, and $M(E)$ is given

by

$$D_L(E) = \frac{|E - E_{d,G}|}{(\pi\hbar v_F)^2} 2[\theta_S + (\theta_S - \theta_D)\vartheta(\theta_S - \theta_D)], \quad (8)$$

$$D_R(E) = \frac{|E - E_{d,G}|}{(\pi\hbar v_F)^2} 2[\theta_D + (\theta_D - \theta_S)\vartheta(\theta_D - \theta_S)], \quad (9)$$

$$M(E) = \min\{M_S(E), M_D(E), M_G(E)\}, \quad (10)$$

where ϑ is the Heaviside step function and

$$M_{S/D/G}(E) = \frac{2W}{\pi} k_{S/D/G}. \quad (11)$$

The numerical value for v_F is set using the equation $v_F = (3/2)a_{CC}|t|/\hbar$, in which $a_{CC} = 1.42 \text{ \AA}$ is the carbon-carbon distance in graphene and $t = -2.7 \text{ eV}$ the tight-binding parameter describing hopping between nearest neighbor p_z orbitals. The quantities $k_{S/D/G}$ and $\theta_{S/D}$ are defined as (their physical meaning is illustrated in Fig. 2-bottom)

$$k_{S/D/G} = \frac{|E - E_{d,S/D/G}|}{\hbar v_F}, \quad (12)$$

$$\theta_{S/D} = \begin{cases} \sin^{-1}(k_{S/D}/k_G) & \text{if } k_{S/D} < k_G, \\ \pi/2 & \text{otherwise.} \end{cases} \quad (13)$$

The Dirac point in the channel $E_{d,G}$ is self-consistently computed with n and p through a plane-capacitor model which accounts for electrostatics:

$$q(n - p) = C_{ox}(-\mu_S/q + V_{GS} + E_{d,G}/q), \quad (14)$$

where C_{ox} is the gate oxide capacitance and a zero workfunction difference is assumed between gate and graphene.

The model in Eqs. 8–13 corresponds to the solution of the ballistic Boltzmann equation in the channel region assuming energy and transverse momentum conservation at the two junctions. As an example, Fig. 2-bottom shows the distribution function in k -space corresponding to the potential in Fig. 2-top and at the indicated energy E . The red/blue (light-gray/dark-gray) color represents $f_{S/D}(E)$. The plot can be understood by assuming that the transmission probability across each junction, for an incident electron with transverse momentum k_y , is either 1, if states with the same k_y are available on the other side of the junction, or 0 otherwise. In the figure, electrons from the source (red or light gray) are perfectly transmitted through both junctions, thus populating only rightward propagating states in the channel (note that the group velocity is opposite to \vec{k} for states in the valence band). The ones from the drain (blue or dark gray) enter the channel with probability one; at the source-channel junction, they are either perfectly transmitted if $|k_y| < k_S$ or totally reflected if $|k_y| > k_S$, thus populating both left- and rightward propagating states.

We highlight the fact that the current contribution at a given energy is determined by the region where the Fermi surface has the smallest radius (Eq. 10), which means a transport bottleneck effect due to the series of graphene junctions. This model for $M(E)$ was first discussed in [24] and was also used to describe NDR in single p-n junction devices [27]. It is worth noting that, if $k_S, k_D > k_G$ (i.e., if the number of modes in the contacts is larger than in the channel), the same model for charge and current as in [12] is recovered.

To benchmark the semianalytical model, we use an atomistic full-quantum code for graphene nanoribbons [28], based on the self-consistent solution of the tight-binding (TB) NEGF and 3D Poisson equations and optionally including graphene acoustic phonon (AP) and optical phonon (OP) scattering. The source and drain regions are treated as in the semianalytical model with a fixed ΔE_{con} and semi-infinite extensions (as in [19]). In the following, we will show results from both ballistic simulations and simulations with phonon scattering; in the latter case, we use the parameters $D_{\omega, \text{AP}} = 0.03 \text{ eV}^2$, $D_{\omega, \text{OP}} = 0.027 \text{ eV}^2$, and $\hbar\omega_{\text{OP}} = 160 \text{ meV}$, whose definitions can be found in [29].

In the semianalytical model presented above, we have assumed that the source and drain regions are described by the same conical electronic dispersion relation as the channel (Eq. 12). In reality, the graphene DOS in the contacted regions is broadened due to the coupling with the metal contacts, so that a finite DOS (and thus a finite current injection) is induced at the Dirac point. In the following, we study separately the effect of contact-induced energy broadening. Regarding the NEGF code, we include the broadening as a constant imaginary diagonal self-energy $-i\Delta$ for the source and drain regions [19]. We have verified that the resulting DOS in the source/drain region, $D_{S/D}(E)$, can be well reproduced by the formula

$$D_{S/D}(E) = 2 \frac{\sqrt{(E - E_{d,S/D})^2 + \tilde{\Delta}^2}}{\pi (\hbar v_F)^2} \quad (15)$$

where $\tilde{\Delta}$ is a fitting parameter. Assuming the same relation between $M_{S/D}$ and $D_{S/D}$ as in the case without broadening,

$$M_{S/D}(E) = D_{S/D}(E) \hbar v_F W, \quad (16)$$

we get an effective dispersion relation

$$k_{S/D} = \frac{\pi}{2W} M_{S/D}(E) = \frac{\sqrt{(E - E_{d,S/D})^2 + \tilde{\Delta}^2}}{\hbar v_F}, \quad (17)$$

which we use in place of Eq. 12 for $k_{S/D}$ to capture the effect of energy broadening within the semianalytical model.

IV. RESULTS

We consider n-type doped source and drain regions (unless stated otherwise, the values $\Delta E_{\text{con}} = 0.4 \text{ eV}$ and $\tilde{\Delta} = \Delta = 0$ are assumed) and an ideal gate dielectric with equivalent oxide thickness (EOT) of 0.5 nm. All the results presented in the following are at room temperature. With $V_{GS} = 0$ and at equilibrium, the channel Dirac point is aligned with the source and drain Fermi levels and the channel is intrinsic; by applying a positive (negative) V_{GS} , the bands in the channel are shifted down (up) thus creating an n-n-n (n-p-n) double junction. We explore in the following both the n-n-n and n-p-n bias conditions.

A. Quasi-saturation in n-n-n structure with $V_{DS} > 0$

In Fig. 3, we plot the output characteristics for $V_{GS} \geq 0$ (n-type channel) from the semianalytical model and the one obtained by setting $k_S, k_D > k_G$ and thus $\theta_S = \theta_D = \pi/2$

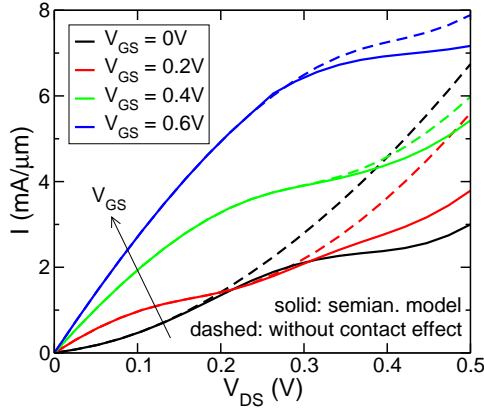


Fig. 3. Normalized output characteristics for $V_{GS} \geq 0$ (n-n configuration) from the semianalytical model (solid line) and the one obtained by assuming $k_S, k_D > k_G$ (dashed line).

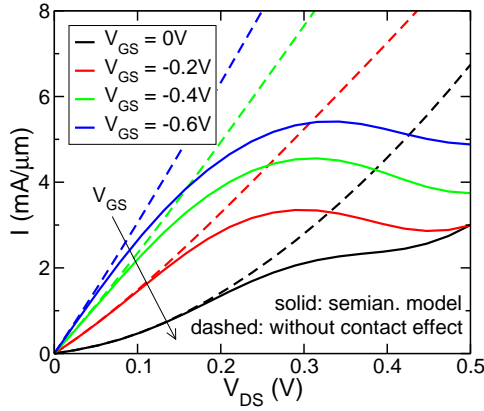


Fig. 4. Normalized output characteristics for $V_{GS} \leq 0$ (n-p-n configuration) from the semianalytical model (solid line) and the one obtained by assuming $k_S, k_D > k_G$ (dashed line).

in Eqs. 8–10 (cfr. [12]). It can be seen that the two models give similar results at large V_{GS} , both predicting the quasi-saturation behavior discussed above. This means that the mode reflection at the two junctions has no significant effect in this bias condition. However, at lower V_{GS} , the two models depart significantly for large V_{DS} . Indeed, at small V_{GS} and large V_{DS} , the channel doping is actually turned p-type by the drain contact and the transport regime is similar to the n-p-n case discussed below.

B. NDR in n-p-n structure with $V_{DS} > 0$

The output characteristics for $V_{GS} \leq 0$ (p-type channel) are shown in Fig. 4. While the model neglecting the finite number of modes in the source and drain predicts a monotonically increasing current, the one proposed here clearly gives NDR.

The origin of the NDR effect is explained by looking at Fig. 5, which compares the band profile, number of modes, and current spectrum (integrand in Eq. 7) obtained at two different V_{DS} biases along the $V_{GS} = -0.4$ V curve. NDR is the combination of two effects. First, for energies close to $E_{d,S}$, $M(E)$ is limited by the number of modes in the source: in particular, for $E = E_{d,S}$ we have $M(E) = 0$, and this leads to the quasi-saturation behavior of the current for μ_D approaching $E_{d,S}$,

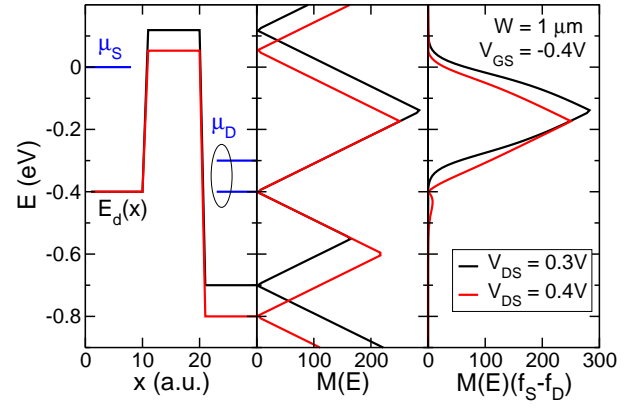


Fig. 5. Dirac point profile (left), number of propagating modes versus energy (center), and current spectrum (right) from the semianalytical model, for two different V_{DS} at $V_{GS} = -0.4$ V.

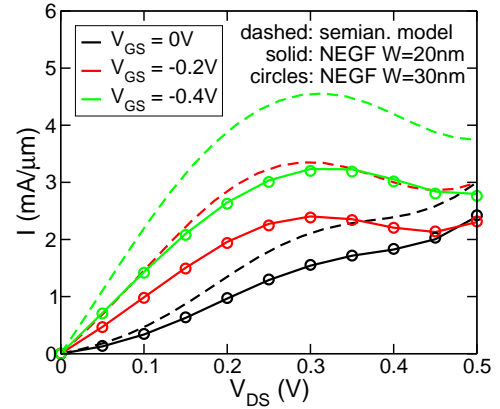


Fig. 6. Normalized output characteristics for $V_{GS} \leq 0$ from the semianalytical model and ballistic NEGF simulations of nanoribbons with two different widths W .

as already pointed out in [19] and mathematically represented (in the zero-temperature approximation) by the first term in the r.h.s. of Eq. 4. Secondly, by lowering μ_D , the flux of electrons injected from the drain into the channel is reduced, while the flux from the source is kept fixed, causing a hole pile-up in the channel: due to the electrostatic feedback, $E_{d,G}$ is lowered and $M(E)$ decreases for a portion of the energy range within μ_S and μ_D , leading to a decrease of the current rather than a saturation, as expressed (in the zero-temperature approximation) by the second term in the r.h.s of Eq. 4. The fact that the decrease in $M(E)$ is not fully compensated by the larger $(\mu_S - \mu_D)$ is confirmed by the plot in Fig. 5-right, where the area under the red curve (current at higher V_{DS}) is slightly smaller than the area under the black curve (current at lower V_{DS}).

We highlight the necessity of two Dirac points, one in the channel and the other one in either the source or the drain, for NDR to be possible instead of saturation. Also, we note that a similar explanation for NDR was given in [18], even if a simple, not self-consistent model for barrier lowering was used (shift of $E_{d,G}$ by $-V_{DS}/2$ with respect to the value at $V_{DS} = 0$).

The qualitative shape of the output characteristics is con-

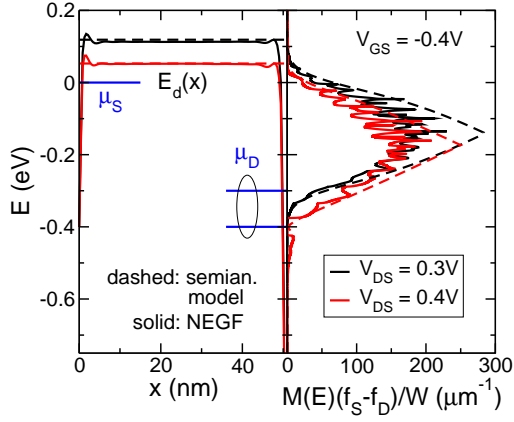


Fig. 7. Dirac point profile (left) and current spectrum (right) from the semianalytical model and from ballistic NEGF simulations for the same two biases as in Fig. 5.

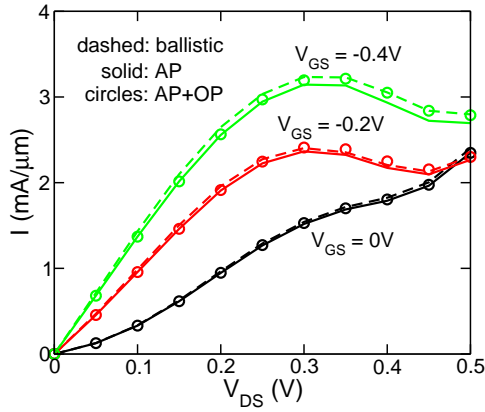


Fig. 8. Normalized output characteristics for $V_{GS} \leq 0$ from NEGF simulations with ballistic transport, with AP scattering, and with both AP and OP scattering.

firmed by ballistic NEGF simulations (Fig. 6) considering a 50-nm-channel length. Since the NEGF code we use is for graphene nanoribbons, we have checked the convergence of the results with respect to the nanoribbon width W : the two sets of NEGF curves for $W = 20$ nm and $W = 30$ nm in Fig. 6 overlap, indicating that the nanoribbons are wide enough to behave as 2D graphene (in real devices, larger widths would be needed to reach the 2D behavior because of the effect of edge roughness).

In Fig. 7 we plot the band profiles and current spectra obtained from the two models. In the ballistic NEGF formalism, the number of propagating modes $M(E)$ in the current expression is replaced by the transmission function $T(E) = \sum_{j=1} T_j(E)$, where $T_j(E)$ is the transmission probability from source to drain of mode j [30]. From the figure, it can be seen that the assumption of square potential barrier is well justified and that the barrier lowering is similar; the lower current spectrum in the NEGF case can be explained with wavefunction mismatch at the junctions, causing $T_j(E) < 1$ for propagating modes even in the case of an abrupt potential step [24], [31].

Finally, we have investigated the effect of scattering due to graphene longitudinal acoustic and optical phonons and found

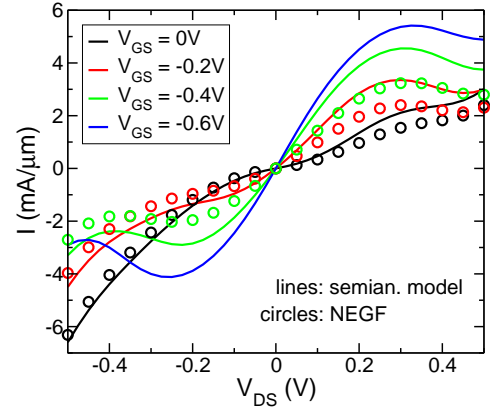


Fig. 9. Normalized output characteristics for $V_{GS} \leq 0$ and for both positive and negative V_{DS} from the semianalytical model and ballistic NEGF simulations.

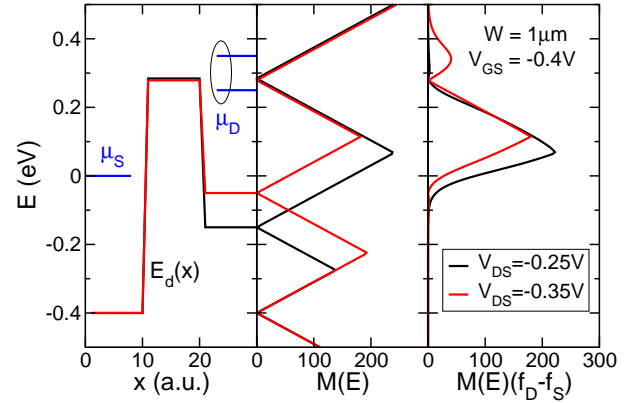


Fig. 10. Dirac point profile (left), number of propagating modes versus energy (center), and current spectrum (right) from the semianalytical model, for two different negative V_{DS} at $V_{GS} = -0.4$ V.

that, at this channel length, it is too weak to affect the current (Fig. 8). Nevertheless, it is worth noting that the effect of OP scattering is to increase slightly the current in the NDR region with respect to the case with only AP scattering: this can be explained by the fact that OP scattering creates additional paths for the current flow due to energy relaxation, thus reducing the transport bottleneck effect induced by $M(E)$.

C. NDR in n-p-n structure with $V_{DS} < 0$

We have also studied the device behavior when the polarity of the drain voltage is reversed. Fig. 9 shows the complete output characteristics for $V_{GS} \leq 0$ including both positive and negative V_{DS} values (the curves for $V_{DS} > 0$ are the same as those shown in Figs. 4 or 6). Another NDR effect, not previously reported, is observed at $V_{DS} < 0$ in both the results of the semianalytical model and NEGF simulations.

To help understand the origin of the phenomenon, we plot in Fig. 10 the band profile and spectra for two negative V_{DS} values along the $V_{GS} = -0.4$ V curve. The mode bottleneck induced by the Dirac point at $E = E_{d,G}$ is responsible for the current saturation as μ_D approaches $E_{d,G}$, since it gives $M(\mu_D) \rightarrow 0$ in Eq. 4. At the same time, when μ_D is raised, the mode bottleneck at $E = E_{d,D}$ causes a decrease of $M(E)$

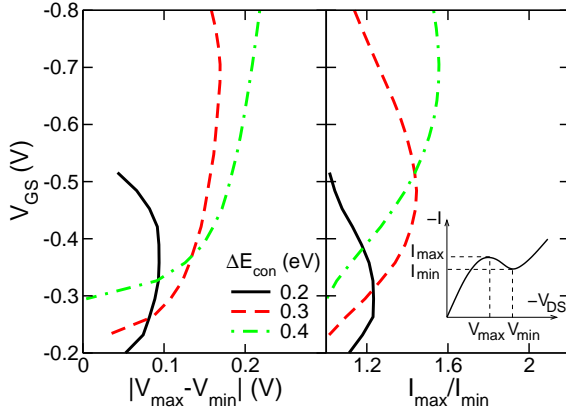


Fig. 11. Dependence on V_{GS} and ΔE_{con} of the voltage swing (left) and peak-to-valley current ratio (right) of NDR at $V_{DS} < 0$. The results are from the semianalytical model. The inset shows the definition of V_{\max} , V_{\min} , I_{\max} , and I_{\min} .

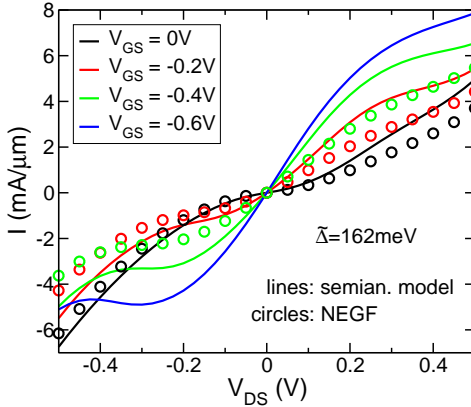


Fig. 12. Normalized output characteristics for $V_{GS} \leq 0$ from the semianalytical model and ballistic NEGF simulations including energy broadening in the source and drain.

within the energy window between μ_S and μ_D , due to the rigid shift of $E_{d,D}$ with μ_D . This corresponds to $\partial M(E)/\partial V_{DS} < 0$ in Eq. 4, so that NDR rather than saturation occurs.

We conclude that the mechanisms for NDR at the two drain voltage polarities are very similar and essentially related to the combined effect of two Dirac points, one in the channel and the other in either the source or the drain, in limiting the current. However, NDR at $V_{DS} < 0$ does not involve an electrostatic feedback in the channel and it is thus expected to be a more robust phenomenon than its counterpart at $V_{DS} > 0$.

While the optimization of NDR is beyond the scope of this work, we just show in Fig. 11 how NDR at $V_{DS} < 0$ can be modulated by varying the electrostatic doping of the contacts, i.e. ΔE_{con} . From the figure, it can be seen that both the voltage swing $|V_{\max} - V_{\min}|$ and the peak-to-valley current ratio I_{\max}/I_{\min} (the symbols are defined in the inset of Fig. 11) can be somewhat enhanced by increasing the contact doping, which also enlarges the V_{GS} window where the phenomenon occurs.

D. Effect of energy broadening in the source and drain regions

To study the effect of energy broadening due to metal-graphene coupling in the source and drain regions, we set

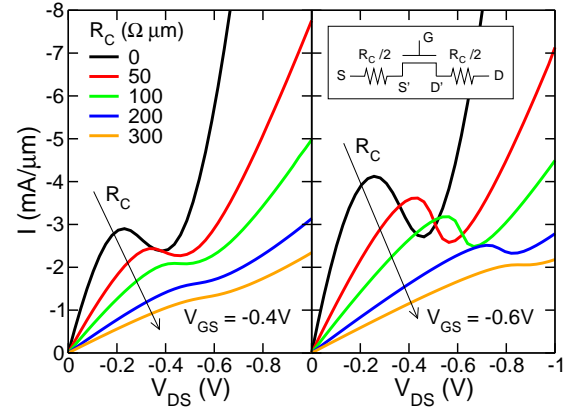


Fig. 13. Normalized output characteristics from the semianalytical model for different values of the contact resistance R_C , at $V_{GS} = -0.4 \text{ V}$ (left) and $V_{GS} = -0.6 \text{ V}$ (right). R_C is split equally between the source and drain terminals as shown in the inset.

$\Delta = 50 \text{ meV}$ in the NEGF code and $\tilde{\Delta} = 162 \text{ meV}$ in the semianalytical model. The latter has been fitted to provide the same value of DOS at the Dirac point, $D_{S/D}(E_{d,S/D}) \approx 3 \times 10^{13} \text{ cm}^{-2} \text{ eV}^{-1}$, as in the NEGF case. The resulting output characteristics are plotted in Fig. 12. The two methods give qualitatively similar results. At $V_{DS} > 0$, NDR disappears as already observed in [19]. However, we find here that NDR, albeit weak, is still possible at $V_{DS} < 0$. The experimental verification of the effect should thus be easier in the $V_{DS} < 0$ case.

E. Effect of contact resistance

We finally consider the effect of a series contact resistance R_C equally split between the source and drain terminals (inset of Fig. 13). The semianalytical model is modified accordingly, by replacing the Fermi level $\mu_{S/D}$ entering the equations for $f_{S/D}$ and $E_{d,S/D}$ with the Fermi level $\mu_{S'/D'}$ of the intrinsic source/drain. The latter is calculated self-consistently with the current I through the resistor equation

$$\mu_{S'/D'} = \mu_{S/D} \mp q \frac{R_C}{2} I, \quad (18)$$

where the upper/lower sign holds for source/drain. The I vs. V_{DS} characteristics for different values of R_C and two values of V_{GS} are shown in Fig. 13. It can be seen that NDR tends to disappear with increasing R_C due to the increasing voltage drop across the two resistors. Already at $R_C = 300 \Omega \cdot \mu\text{m}$, which is a typical experimental value [14], the output curve resembles the linear characteristic of a resistor, for both values of the gate voltage considered, indicating that contact resistance is a major problem for the operation of short-channel devices.

V. DISCUSSION

The analysis above indicates that, given a specific type of doping of the contacted graphene regions, the gate voltage needs to be biased such that an n-p-n or p-n-p double junction is formed, in order for NDR in ballistic GFETs to be possible. In addition, NDR is expected to be more likely for drain

voltages with the same polarity as V_{GS} , due to the higher robustness of NDR against energy broadening in this case. It is interesting to compare these findings with the actual bias conditions employed in experiments to observe NDR.

We note that the long-channel devices in [14], [15] were biased in an n-n-n or p-p-p configuration thus ruling out our interpretation of the phenomenon. Indeed, for channel lengths of the order of $1\mu\text{m}$, scattering is expected to cause significant momentum and energy relaxation and charge inhomogeneity along the channel, so that the drift-diffusion interpretation discussed in Section II seems more appropriate.

On the other hand, in the Supporting Information of [14], results for GFETs with channel lengths of about 100 nm have been reported too. Some of these devices show NDR for gate voltages around 0 V: this biasing could be the counterpart case of the one mentioned at the end of Section IV-A, (incompletely formed p-type channel, p-type contacts, and $V_{DS} < 0$), so that our explanation of NDR could apply in this case. However, further experimental evidence is needed to prove this hypothesis (for example by exploring all the V_{GS} and V_{DS} polarities).

VI. CONCLUSIONS

Through a semianalytical model and detailed quantum simulations, we have clarified the nature and bias conditions for NDR in short-channel GFETs. The origin of the phenomenon is attributed to the transport-mode bottleneck induced by the graphene Dirac point. The combined effect of two Dirac points, one in the channel and the other in either the source or the drain, is necessary for NDR to occur instead of quasi-saturation. This is verified in the n-p-n or p-n-p configuration, for both polarities of V_{DS} . In the presence of energy broadening due to the metal-graphene coupling in the source and drain regions, NDR disappears at one V_{DS} polarity, but a weak NDR, or at least saturation, is still attainable at the other one. It is also found that contact resistance at typical experimental values suppresses NDR, representing a major obstacle for the verification of the phenomenon in experiments.

The NDR mechanism could offer new possibilities for the optimization of the saturation behavior of the output characteristics of analog GFETs. The semianalytical model presented here, providing a good physical insight of NDR, could be a useful simulation tool for such an optimization study.

ACKNOWLEDGMENT

The authors would like to thank Dr. Y. Wu, IBM T. J. Watson Research Center, Yorktown Heights, NY, for fruitful discussions about the interpretation of the results. This work has been supported by the Italian Project PRIN 2008 prot. 2008S2CLJ9. The authors acknowledge the CINECA Award N. HP10CPFJ69, 2011 for the availability of high performance computing resources and support.

REFERENCES

- [1] I. Meric, N. Baklitskaya, P. Kim, and K. L. Shepard, "RF performance of top-gated, zero-bandgap graphene field-effect transistors," in *Int. Electron Devices Meeting Tech. Dig.*, 2008, pp. 1–4.
- [2] L. Liao, Y.-C. Lin, M. Bao, R. Cheng, J. Bai, Y. Liu, Y. Qu, K. L. Wang, Y. Huang, and X. Duan, "High-speed graphene transistors with a self-aligned nanowire gate," *Nature*, vol. 467, no. 7313, pp. 305–308, 2010.
- [3] Y.-M. Lin, C. Dimitrakopoulos, K. A. Jenkins, D. B. Farmer, H.-Y. Chiu, A. Grill, and P. Avouris, "100-GHz transistors from wafer-scale epitaxial graphene," *Science*, vol. 327, no. 5966, p. 662, 2010.
- [4] Y. Wu, Y. ming Lin, A. A. Bol, K. A. Jenkins, F. Xia, D. B. Farmer, Y. Zhu, and P. Avouris, "High-frequency, scaled graphene transistors on diamond-like carbon," *Nature*, vol. 472, no. 7341, pp. 74–78, 2011.
- [5] F. Schwierz, "Graphene transistors," *Nature Nanotechnology*, vol. 5, pp. 487–496, 2010.
- [6] Y.-M. Lin, A. Valdes-Garcia, S.-J. Han, D. B. Farmer, I. Meric, Y. Sun, Y. Wu, C. Dimitrakopoulos, A. Grill, P. Avouris, and K. A. Jenkins, "Wafer-scale graphene integrated circuit," *Science*, vol. 332, no. 6035, pp. 1294–1297, 2011.
- [7] I. Meric, M. Y. Han, A. F. Young, B. Ozyilmaz, P. Kim, and K. L. Shepard, "Current saturation in zero-bandgap, top-gated graphene field-effect transistors," *Nature Nanotechnology*, vol. 3, pp. 654–659, 2008.
- [8] J. Bai, L. Liao, H. Zhou, R. Cheng, L. Liu, Y. Huang, and X. Duan, "Top-gated chemical vapor deposition grown graphene transistors with current saturation," *Nano Letters*, vol. 11, no. 6, pp. 2555–2559, 2011.
- [9] S.-J. Han, K. A. Jenkins, A. V. Garcia, A. D. Franklin, A. A. Bol, and W. Haensch, "High-frequency graphene voltage amplifier," *Nano Letters*, vol. 11, no. 9, pp. 3690–3693, 2011.
- [10] S. A. Thiele, J. A. Schaefer, and F. Schwierz, "Modeling of graphene metal-oxide-semiconductor field-effect transistors with gapless large-area graphene channels," *J. Appl. Phys.*, vol. 107, no. 9, p. 094505, 2010.
- [11] D. Jiménez and O. Moldovan, "Explicit drain-current model of graphene field-effect transistors targeting analog and radio-frequency applications," *IEEE Trans. Electron Devices*, vol. 58, no. 11, pp. 4049–4052, 2011.
- [12] S. O. Koswatta, A. Valdes-Garcia, M. B. Steiner, Y.-M. Lin, and P. Avouris, "Ultimate RF performance potential of carbon electronics," *IEEE Trans. Microw. Theory Tech.*, vol. 59, no. 10, pp. 2739–2750, 2011.
- [13] K. Ganapathi, M. Lundstrom, and S. Salahuddin, "Can quasi-saturation in the output characteristics of short-channel graphene field-effect transistors be engineered?" in *Proc. Device Research Conf.*, University Park, PA, Jun. 2012, pp. 85–86.
- [14] Y. Wu, D. B. Farmer, W. Zhu, S.-J. Han, C. D. Dimitrakopoulos, A. A. Bol, P. Avouris, and Y.-M. Lin, "Three-terminal graphene negative differential resistance devices," *ACS Nano*, vol. 6, no. 3, pp. 2610–2616, 2012.
- [15] S.-J. Han, D. Reddy, G. D. Carpenter, A. D. Franklin, and K. A. Jenkins, "Current saturation in submicrometer graphene transistors with thin gate dielectric: Experiment, simulation, and theory," *ACS Nano*, vol. 6, no. 6, pp. 5220–5226, 2012.
- [16] Y. Wu, V. Perebeinos, Y.-M. Lin, T. Low, F. Xia, and P. Avouris, "Quantum behavior of graphene transistors near the scaling limit," *Nano Lett.*, vol. 12, no. 3, pp. 1417–1423, 2012.
- [17] D. Dragoman and M. Dragoman, "Negative differential resistance of electrons in graphene barrier," *Appl. Phys. Lett.*, vol. 90, no. 14, p. 143111, 2007.
- [18] V. N. Do, V. H. Nguyen, P. Dollfus, and A. Bournel, "Electronic transport and spin-polarization effects of relativistic-like particles in mesoscopic graphene structures," *J. Appl. Phys.*, vol. 104, no. 6, p. 063708, 2008.
- [19] P. Zhao, Q. Zhang, D. Jena, and S. O. Koswatta, "Influence of metal-graphene contact on the operation and scalability of graphene field-effect transistors," *IEEE Trans. Electron Devices*, vol. 58, no. 9, pp. 3170–3178, 2011.
- [20] R. Grassi, T. Low, A. Gnudi, and G. Baccarani, "Negative differential resistance in short-channel graphene FETs: semianalytical model and simulations," in *Proc. Device Research Conf.*, University Park, PA, Jun. 2012, pp. 107–108.
- [21] V. Perebeinos and P. Avouris, "Inelastic scattering and current saturation in graphene," *Phys. Rev. B*, vol. 81, p. 195442, 2010.
- [22] J. Tworzydło, B. Trauzettel, M. Titov, A. Rycerz, and C. W. J. Beenakker, "Sub-poissonian shot noise in graphene," *Phys. Rev. Lett.*, vol. 96, p. 246802, 2006.
- [23] Y. Sui, T. Low, M. Lundstrom, and J. Appenzeller, "Signatures of disorder in the minimum conductivity of graphene," *Nano Lett.*, vol. 11, p. 1319, 2011.

- [24] T. Low, S. Hong, J. Appenzeller, S. Datta, and M. S. Lundstrom, "Conductance asymmetry of graphene p-n junction," *IEEE Trans. Electron Devices*, vol. 56, no. 6, pp. 1292–1299, 2009.
- [25] V. V. Cheianov and V. I. Falko, "Selective transmission of dirac electrons and ballistic magnetoresistance of n-p junctions in graphene," *Phys. Rev. B*, vol. 74, p. 041403R, 2006.
- [26] G. Giovannetti, P. A. Khomyakov, G. Brocks, V. M. Karpan, J. van den Brink, and P. J. Kelly, "Doping graphene with metal contacts," *Phys. Rev. Lett.*, vol. 101, p. 026803, 2008.
- [27] G. Fiori, "Negative differential resistance in mono and bilayer graphene p-n junctions," *IEEE Electron Device Lett.*, vol. 32, no. 10, pp. 1334–1336, 2011.
- [28] I. Imperiale, R. Grassi, A. Gnudi, S. Reggiani, E. Gnani, and G. Bacarani, "Full-quantum calculations of low-field channel mobility in graphene nanoribbon FETs including acoustic phonon scattering and edge roughness effects," in *Proc. ULIS*, Glasgow, UK, Mar. 2010, pp. 57–60.
- [29] Y. Yoon, D. E. Nikonov, and S. Salahuddin, "Role of phonon scattering in graphene nanoribbon transistors: Nonequilibrium Green's function method with real space approach," *Appl. Phys. Lett.*, vol. 98, no. 20, p. 203503, 2011.
- [30] S. Datta, *Electronic Transport in Mesoscopic Systems*. Cambridge, UK: Cambridge University Press, 1997.
- [31] M. I. Katsnelson, K. S. Novoselov, and A. K. Geim, "Chiral tunnelling and the Klein paradox in graphene," *Nature Phys.*, vol. 2, pp. 620–625, 2006.